

Integrated Modeling Methodology Validation Using the Micro-Precision Interferometer Testbed: Assessment of Closed Loop Performance Prediction Capability

James W. Melody
jmelody@csi.jpl.nasa.gov
(818) 354 0615

Gregory W. Neat
neat@huey.jpl.nasa.gov
(818) 354-0611

Jet Propulsion Laboratory,
California Institute of Technology
4800 Oak Grove Drive
Pasadena, CA 91109

Abstract

This paper validates the integrated modeling methodology used for design and performance evaluation of complex opto-mechanical systems, particularly spaceborne interferometers. The methodology integrates structural modeling, optical modeling, and control system design into a common environment, the Integrated Modeling of Optical Systems (IMOS) software package. The validation utilized the Micro-Precision Interferometer (MPI) testbed, a ground-based full-scale hardware model of a spaceborne interferometer. Parallel development of the MPI testbed and the MPI IMOS model enabled a unique opportunity to validate the modeling methodology with actual hardware measurements from the testbed. This paper assesses the ability of the integrated modeling methodology to predict performance in a closed loop configuration; namely with the high bandwidth optical control loops operational. This paper presents a comparison of integrated model closed loop predictions with MPI laboratory closed loop measurements, indicating that the integrated modeling methodology has the accuracy required to evaluate interferometry mission designs with confidence.

1 Introduction

Spaceborne optical interferometers provide the only feasible method to significantly improve the angular resolution and astrometric accuracy of current astronomical telescopes such as the Hubble Space Telescope (1.5" resolution). This partial-aperture approach offers a number of important advantages over the traditional full-aperture approach including: control of systematic errors, a significantly lighter instrument yielding the same performance, and improved performance for

a given amount of collecting area. However, this approach requires positional stability of optical elements down to the nanometer level as well as laser metrology resolution to the picometer level [1, 2]. Achieving these control and sensing requirements is particularly difficult because the instrument consists of many optical elements distributed across a 10-m flexible truss structure. To further complicate the problem, the structure is excited by mechanical disturbances emanating predominantly from the attitude control system actuators.

The charter for the Jet Propulsion Laboratory Interferometer Technology Program is to mitigate risk for this optical-interferometer mission class [3]. A number of ongoing complementary activities address these challenges including: integrated modeling methodology development and validation, hardware metrology testbeds, hardware vibration testbeds, and flight qualification of the interferometer components. Though all of these activities are necessary to buy down mission risk, it is integrated modeling that ultimately will be used in the mission and instrument design. Specifically, modeling will enable definition and flow down of spacecraft/instrument requirements, performance of spacecraft/instrument design trades, and prediction of instrument performance in the anticipated on-orbit disturbance environment. This paper investigates whether the integrated modeling methodology has the necessary capability to meet these demanding analysis needs.

In anticipation of these needs, the Integrated Modeling of Optical Systems (IMOS) and the Controlled Optics Modeling Package (COMP) software packages were developed at JPL [5, 6]. The integrated modeling methodology combines structural modeling, optical modeling, and control system design within a common software environment, using these packages. The en-

able validation of the methodology, its development intentionally coincided with the phased delivery of the Micro-Precision Interferometer testbed (MPI).

The MPI testbed is a ground-based, suspended hardware model of a future space-based interferometer located at JPL [7, 8, 9]. The primary objective of the testbed is integration of the vibration attenuation technologies required to demonstrate the end-to-end operation of a space-based interferometer. Figure 1 shows a bird's-eye view of the test bed which contains all systems necessary to perform a space-based, optical-interferometry measurement. These systems include a 7.111 x 6.5 m softly suspended truss structure with mounting plates for subsystem hardware, a six-axis vibration isolation system which supports a reaction wheel assembly to provide a flight-like input disturbance source, a complete Michelson interferometer with high-bandwidth optical control systems, internal and external metrology systems, and a state simulator that injects the "stellar" signal into the interferometer collecting apertures.

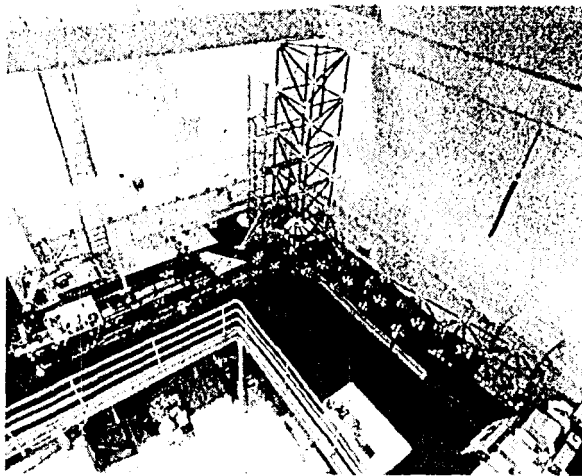


Figure 1: Bird's-eye view of the MPI Testbed.

An integrated model of MPI was CICVC101XX1 in parallel with the test bed. This modeling/hardware synergy resulted in a unique opportunity to validate the modeling methodology by comparing model predictions with testbed measurements. Of the three functions required from the modeling methodology (performance prediction, requirements definition, and design trades), performance prediction was initially deemed the most critical validation, due to the associated nanometer-level positional stability requirements. As such, this paper reports validation of the integrated modeling methodology by comparing predicted and measured performance metrics.

Exhaustive model and test bed comparisons for all instrument disturbance configurations including: (1) hard mounted

disturbance source/open loop optical system, (2) hard mounted disturbance source/closed loop optical system and (3) isolated disturbance source/closed loop optical system. Problem (1) has been previously addressed on the testbed [4]. This paper addresses problem (2) by presenting the closed loop performance validation procedure, the optical control problem, the closed loop MPI integrated model, and the validation results.

2 Validation Procedure

Figure 2 presents the integrated modeling methodology validation procedure for the closed loop optical control system configuration. The figure classifies each step as either a hardware procedure or an analysis procedure. The model is initially built (step 1) using knowledge of the structure geometry, optical layout, etc. The structural parameters are updated (step 3) based on modal test data acquired from the testbed (step 2). Steps (1), (2) and (3) have been presented extensively in the literature [1, 2].

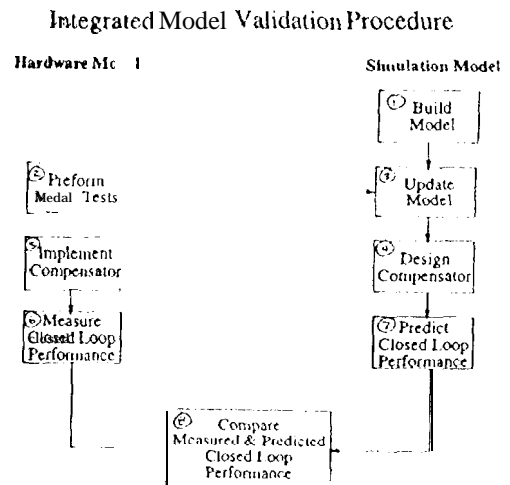


Figure 2: Integrated modeling methodology validation procedure.

Step (4) involves designing the optical control system using the integrated model. Predicted plant transfer functions are used to perform the control system design. Design considerations include practical implementation issues such as the effect of sampling delays, quantization errors, actuator and sensor dynamic range limitations, and reasonable filter order. This compensator is then implemented in the laboratory on the actual hardware (step 5). (state assumptions about sensor/actuator model fidelity)

Disturbance transfer functions from disturbance input location to optical output location are used to assess

system performance. These transfer functions are measured in the laboratory (step 6) and predicted using the closed loop integrated model (step 7). Finally, these results are compared using metrics (step 8) as defined in [4]. (maybe add plant transfer function comparison of a performance/stability sensitivity plot to assess robustness to compensator parameter [r] changes)

3 Fringe Tracker Control Problem

The purpose of the fringe tracking control system is to equalize stellar pathlength from the target star through each arm of the interferometer to the point they are combined. The fringe tracking must nominally stabilize this optical path difference down to 10 nm (1/30 NIS). Figure 3 shows a basic block diagram of the fringe tracking control system.

MPJ TESTBED FRINGE TRACKER BLOCK DIAGRAM

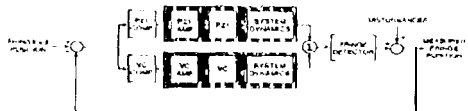


Figure 3: Block diagram of the fringe tracker control system.

The actuator for this subsystem is the active delay line which actually consists of three nested actuators. This three-tiered actuator acts as a linearly translating retroreflector with tremendous dynamic range. A stepper motor provides low frequency (dc), long travel capability (m). An intermediate voice coil actuator translates (cm) the entire cat's eye assembly in the mid-frequency range (dc-100 Hz). A re-actuated piezo supporting the secondary mirror provides the high bandwidth (kHz) precise actuation stage (μm). The coarse stepper motor stage is used primarily to slew and acquire a new stellar fringe. Once acquired, this stage is locked down and the other two stages provide the actuation necessary to reject disturbances during an observation.

The sensor for this system is the fringe detector. This optical sensor measures the amplitude and phase of the stellar fringe down to the nanometer-level.

References [10], [11] describe the control design procedures for this system. The top-level requirements are: (maybe this should all be referenced).

- maximize feedback at low frequency
- cross-over at or below 100 Hz

- disturbance description

This paper applies these design procedures to the integrated model. Special consideration is given to practical implementation issues.

4 Integrated Modeling

Integrated modeling is performed with two software packages: Integrated Modeling of Optical Systems (IMOS) [5] and the Controlled Optics Modeling Package (COMP) [6]. Both packages have been developed at the Jet Propulsion Laboratory. IMOS is a set of functions that run within the MATLAB environment [12], whereas COMP is a stand-alone, FORTRAN-compiled program. A commercial version of COMP is available under the name MACOS (Modeling and Analysis of Controlled Optical Systems).

IMOS is a collection of MATLAB M-files that can be used to perform structural finite element modeling and analysis, optical ray tracing, and thermal analysis. IMOS also provides graphics functionality that enables viewing of structural geometries, structural deformations, optical ray traces, and optical element prescriptions. The core programs are easily coupled in MATLAB, and can be extended by the user by writing his own MATLAB functions. MATLAB toolboxes for control system design and analysis, signal processing, and optimization are available for enhancing the capability of IMOS. Detailed optical and thermal analysis are accommodated in IMOS by interfaces with COMP, and TRASYS and SINDA (for thermal analysis). The interface with COMP has been made effortless by creating a MATLAB r[lex-file version of MACOS. The result is an extremely flexible tool that enables the user to integrate models from different disciplines and conduct analysis, design, and optimization trades that would otherwise be exceedingly difficult [5].

COMP is an optical analysis and modeling program, providing geometric ray-trace, differential ray-trace, and diffraction modeling capability. COMP concentrates on providing detailed optical models for integrated design and analysis tasks. In particular, the differential ray-trace capability of Cohn can be used to generate linear perturbation models of optical systems [6].

5 MPJ Integrated Model

The MPJ integrated model consists of a structural finite element model and a linear optical model that are integrated together. The structural model is generated with IMOS, whereas both IMOS and COMP are

used to create the optical model. The integration, control system modeling, and disturbance analysis are performed in MATLAB with the aid of IMOS functions.

5.1 Structural Model

The structural model is specified in IMOS as a finite element geometry, shown in Figure 4. This geometry consists of plate, beam, truss, and rigid body elements, modeling the base truss structure and the components. The base truss structure is made up of tilt (T) booms: the horizontal optics boom, the vertical tower, and the canted metrology boom. The components consist of in-board and out-board optics plates, a disturbance mount plate, two siderostat mounts, an optics cart containing an active delay line, the optics cart support structure, a hexapod isolation system, a passive delay line, and an external metrology beam launcher plate. The finite element model uses 2,577 degrees of freedom (DOF) of which 1,832 dofs are independent with respect to the multi-point constraints (MPCs) of the rigid body elements (Rims) [5].

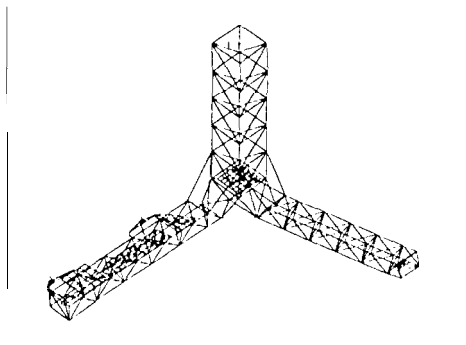


Figure 4: MPI Finite Element Geometry (compare with Figure 1).

Since the focus of this effort is to validate the integrated modeling methodology, it is important to have a structural model with accurate properties. If this input to the integrated modeling methodology is incorrect, then the validation results would be poor regardless of the accuracy of the modeling methodology. For this reason, the plate and beam properties as well as the finite element geometry itself have been refined by incorporating MPI modal test data into the model. The structural model updating has been done in two phases, following the phased delivery of the MPI testbed. The first phase involved estimating the parameters of the beams comprising the base truss structure from modal testing performed on the bare truss [13, 14]. The second phase involved geometry modification and parameter estimation of the optics cart support structure, using *in situ* component modal test data [15, 16].

From the finite element geometry and its associated properties the system mass and stiffness matrices are

built. The result is a second-order, state-space description of the form:

$$M\ddot{d} + Kd = B_f f \quad (1)$$

where M and K are the system mass and stiffness matrices, d is the nodal state, f is a vector of force input, and B_f is the force influence matrix.

After the system mass and stiffness matrices are built, multi-point constraints are generated using RBE elements. These constraints take the form of [5]:

$$d = \begin{bmatrix} d_n \\ d_m \end{bmatrix} = \begin{bmatrix} I_n \\ G_m \end{bmatrix} d_n = Gd_n \quad (2)$$

where d_n are the independent degrees of freedom and d_m are the dependent degrees of freedom. These constraints are then applied to Equation 1, reducing the State of the system to the independent degrees of freedom:

$$\begin{aligned} G^T M G \ddot{d}_n + G^T K G d_n &= G^T B_f f \\ M_{nn} \ddot{d}_n + K_{nn} d &= B_{nf} f \end{aligned} \quad (3)$$

The eigensolution of Equation 3 is found, yielding flexible-body modes and modeshapes. The resultant diagonalized system is:

$$\begin{aligned} \ddot{\eta} + 2Z\Omega\dot{\eta} + \Omega^2\eta &= \Phi_n^T B_{nf} f \\ (1 &= G\Phi_n\eta) \end{aligned} \quad (4)$$

where η is the modal state vector, Z is a diagonal modal damping matrix, Ω is the diagonal modal frequency matrix, and Φ_n is the eigenvector matrix. Z is formed by assuming a modal damping of 0.3% for flexible body modes above 32 Hz and damping ranging from 0.15% to 0.45% for modes below 32 Hz. These damping values correspond to estimates obtained from the second phase of modal tests.

5.2 Optical Model

The optical model begins with a specification of the optical prescription. This prescription includes the shapes, positions, and orientations of the optical elements. A ray trace of the optical prescription is shown in Figure 5. This optical prescription is generated in IMOS based on the prescription of the actual optical elements of MPI (see Figure (i)). The model generation uses the Structural finite element geometry in order to simplify the prescription definition and to ease the succeeding structural-optical model integration. This allows the location of the actual optical elements to be measured with respect to reference points on the structure as opposed to with each other. Furthermore, structural nodes that correspond to optical element attachment points are easily identified and defined.

Once the optical prescriptions are specified, they are exported to COMP, where linear optical models are created. These linear models are calculated by performing an analytic differential ray trace [6]. The result is a model of the form:

$$y = C_{opt}d \quad (5)$$

where d is a vector of optical element position and orientation perturbations, y is a vector of optical output, and C_{opt} is the optical sensitivity matrix. The optical output can be pathlength, wavefront tilt, or spot motion.

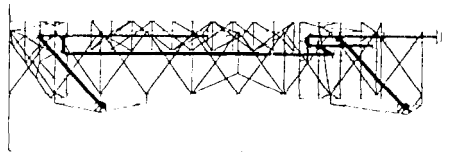


Figure 5: Ray trace of the MPI optical prescription on the finite element geometry of the optics boom.

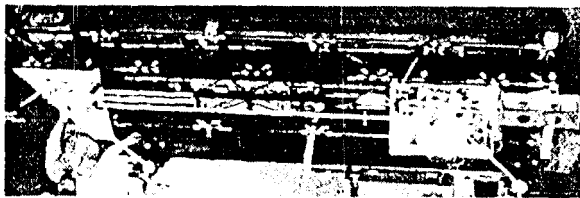


Figure 6: Actual optical layout on the MPI optics boom.

5.3 Structural-Optical Model Integration

Once the structural modal model and the linear optical model have been created, they are integrated to form a structural-optical model. This integrated model is specified in first-order, state-space form, lending itself most easily to analysis with existing MATLAB functions. In particular, the state-space integrated model can be used for frequency-domain analysis, time-domain simulation, and closed-loop synthesis.

First, the structural model is truncated to remove modes above the bandwidth of expected disturbances (i. e., above 900 Hz) [17, 18]. The truncated modal model is then converted into first-order, state-space form by using the substitution [5]:

$$\dot{x} = \begin{bmatrix} \eta_k \\ \dot{\eta}_k \end{bmatrix} \quad (6)$$

Resulting in:

$$\begin{aligned} \dot{x} &= Ax + Bu \\ d &= C_d x + Du \end{aligned} \quad (7)$$

with:

$$\begin{aligned} A &= \begin{bmatrix} 0 & I \\ -2Z_k\Omega_k & -\Omega_k^2 \end{bmatrix} & B &= \begin{bmatrix} 0 \\ \Phi_{nk}^T G^T B_f \end{bmatrix} \\ C_d &= \begin{bmatrix} G\Phi_{nk} & 0 \\ 0 & G\Phi_{nk} \end{bmatrix} & D &= 0 \end{aligned} \quad (8)$$

where the subscript k refers to the set of kept mode-shapes.

Finally, the linear optical model is incorporated into the first-order model. The optical output is obtained by premultiplying d by the optical sensitivity matrix, C_{opt} . In this case the matrix C of the measurement equation of Equation 7 becomes:

$$C = C_{opt}C_d \quad (9)$$

Note that the matrix D of Equation 7 is still zero but now has different dimension.

5.4 Optical Control System Model

Given the integrated structural-optical model in first-order state-space form, the optical control synthesis and modeling are performed with MATLAB Control System Toolbox functions.

6 MPI Testbed

6.1 Compensator Implementation

6.2 Performance Measurements

The MPI testbed is dedicated to the development and evaluation of vibration attenuation technologies. In part, this evaluation consists of observing the improvement in interferometer performance due to the application of the various technologies. Interferometer performance is primarily degraded by variation in optical pathlength difference (OPD), i.e., the difference in the distances that the light travels from the stellar source, through each arm of the interferometer to the interference optical detector. This difference must be stabilized to the 10 nm (RMS) level in the on-orbit mechanical disturbance environment [2].

In contrast to estimating modal characteristics as in [15, 16], disturbance input to stellar OPD output transfer functions were measured since they completely characterize (in a linear sense) the propagation of disturbances to OPD. Figure 7 shows the disturbance input location relative to the OPD output location for the MPI testbed. This disturbance transfer function was measured for three force disturbance directions: (x, y, z). An HP data analyzer was used to collect the data. A 10 h' shaker, mounted at the base of the tower, applied the force input in each of the three directions. The force input was measured with a load cell mounted between the shaker and the structure. The analyzer calculated the transfer function from force input to OPD output.

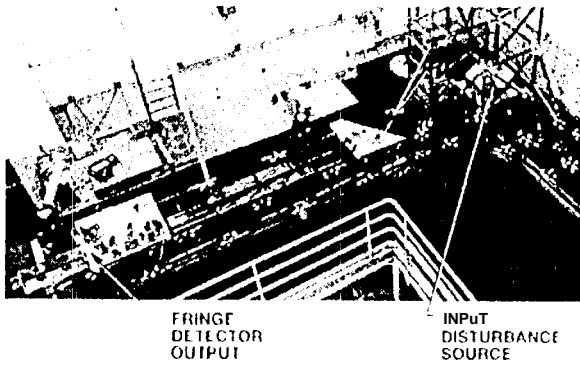


Figure 7: Locations of disturbance input and OPD output on the MPI testbed.

7 Comparison Metric and Results

In general on space-based interferometers, mechanical disturbances will be either broadband or narrowband with the energy varying over broad frequency ranges as a function of time [17, 18]. In either case, the power spectral density of the disturbance is broadband. Therefore, the integrated model should be accurate in a broadband sense. More specifically, we desire σ_{opd} to be accurate, where [19]:

$$\sigma_{opd}^2 = \frac{1}{\pi} \int_{f_{min}}^{f_{max}} |G(j\omega)|^2 \Phi_d(\omega) d\omega \quad (10)$$

for a broadband disturbance power spectral density, $\Phi_d(\omega)$, and a disturbance to OPD transfer function, $G(j\omega)$

Since Equation 10 yields the quantity that we wish to accurately predict, we can use this same equation as a metric to characterize the measured and predicted transfer functions. As opposed to picking a particular expected disturbance power spectral density, bandlimited white noise (over $[f_{min}, f_{max}]$) is used:

$$\sigma_g^2 = \frac{A_d}{\pi} \int_{f_{min}}^{f_{max}} |G(j\omega)|^2 d\omega \quad (11)$$

where A_d is the amplitude of the bandlimited white noise disturbance power spectral density with f_{min} and f_{max} defining the frequency range of interest. σ_g is used instead of σ_{opd} in order to stress that the result is a metric of the transfer function itself.

Using this metric, the accuracy of the model can be quantified by comparing σ_g for the predicted and measured transfer functions. As such, the particular value of the disturbance amplitude is immaterial. The amplitude is chosen so that the variance of the disturbance is one. This choice is arbitrary, and the value of σ_g has no significance by itself. It is the comparison of the metrics for corresponding measured and predicted

transfer functions that is meaningful. Generally, it is desired that OPD variation predictions be accurate to within a factor of 4. Since the metric σ_g is closely related to OPD variations for broadband noise, the factor of 4 is applied as a requirement to the ratio of σ_g for the measured and predicted transfer functions.

The modulus of the measured transfer functions, along with the corresponding predicted transfer functions, are shown in Figures 8-10. The predicted transfer functions were calculated by applying standard MATLAB functions to the integrated model with disturbance force input and OPD output. The value of the broadband metric, also calculated with MATLAB functions, is given in the legend for each transfer function.

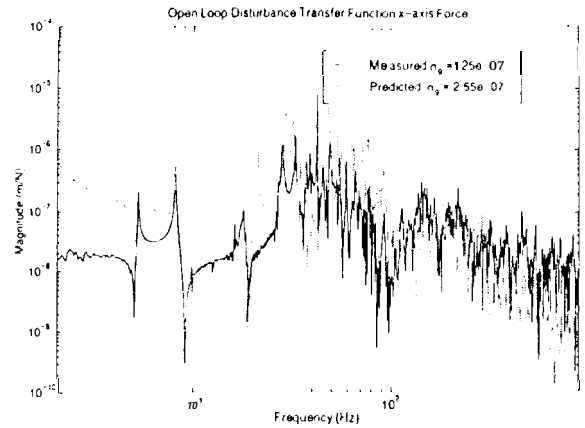


Figure 8: Predicted and measured MPI disturbance to OPD transfer function: x-axis force input.

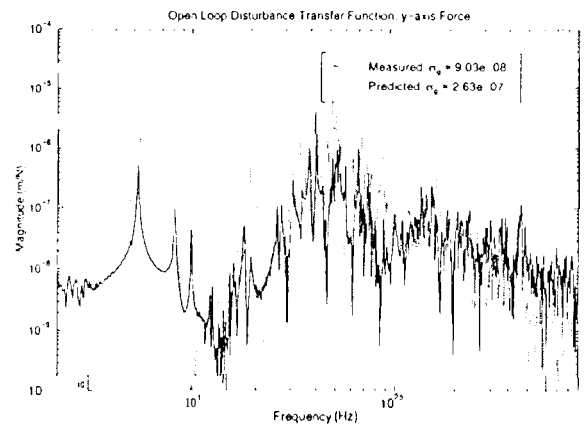


Figure 9: Predicted and measured MPI disturbance to OPD transfer function: y-axis force input.

The results of these comparisons are shown in Table 1. The bandwidth of interest is [4, 900] Hz. Below 4 Hz the force capability of the shaker is limited and the testbed suspension modes pollute the measurement. Above 900 Hz the mechanical disturbances are expected to have no energy. This bandwidth is further broken roughly into decades and comparisons are

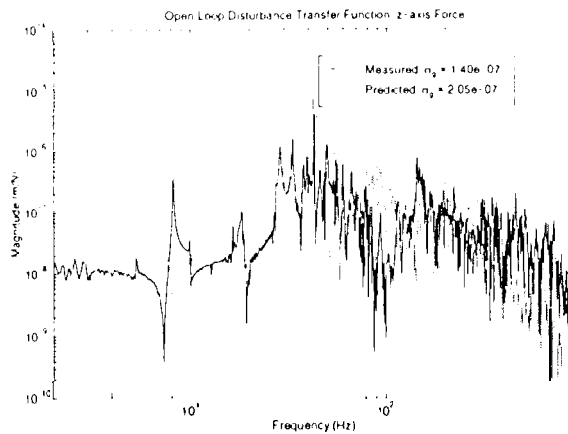


Figure 10: Predicted and measured MPI disturbance to OPD transfer function: z-axis force input.

shown for these “decades.” Units are not given in the table so as to discourage the reader from attaching significance to the separate values.

The comparisons for the three form disturbance transfer functions show that the broadband metrics ([4, 900] Hz) for the predicted transfer functions are accurate with respect to the measured transfer functions to well within the desired factor of four. Furthermore, the comparisons for each “decade” show accuracies of better than a factor of four. This indicates that OPD variation estimates for colored broadband input should also be accurate.

Disturbance Input		4 - 10 Hz	10 - 100 Hz	100 - 900 Hz	4 - 900 Hz
x-axis Force	meas	7	117	43	125
	pred	13	253	31	255
	factor	1.91	2.15	0.73	2.04
y-axis Force	meas	5	84	32	90
	pred	19	260	35	263
	factor	3.57	3.08	1.11	2.92
z-axis Force	meas	4	117	76	140
	pred	4	194	67	205
	factor	1.02	1.65	0.87	1.47

Table 1: Broadband transfer function metric comparison between the predicted and measured transfer functions of the MPI Testbed.

8 Conclusion/Future Work

This paper validates the performance prediction capabilities of the integrated modeling methodology which incorporates the IMOS and COMP analysis tools. A metric is proposed that characterizes the disturbance

transfer functions over a broad frequency range. This metric is simply the expected OPD variation assuming a bandlimited white noise disturbance input. Comparisons between predicted and measured transfer function metrics show that the model is accurate to within a factor of 3.0 over the frequency range of interest, [4, 900] Hz. This is comfortably better than the desired factor of four. Furthermore, comparisons of the metric applied over each decade in the frequency range show an accuracy to within a factor of four. This indicates that performance predictions for colored broadband input should also be accurate.

However, this study only addressed the hard-mounted-disturbance, active-optics configuration. Validation results have previously been reported for the hard-mounted, open-loop configuration [4]. Ongoing activities include validation of the methodology for passive and active vibration isolation, inclusion of disturbance torque transfer functions in the validation, and assessment of the sensitivity of these results to the accuracy of the structural model.

References

- [1] M. Shao, “Orbiting Stellar Interferometer,” Proceedings of the SPIE Symposium on OE/Aerospace, Science and Sensing, Conference on Spaceborne Interferometry, vol. 1947, pp. 89, Orlando, FL, April 1993.
- [2] M. Shao and D. M. Wolf, “Orbiting Stellar Interferometer,” Proceedings of the SPIE Symposium on OE/Aerospace, Science and Sensing, Conference on Spaceborne Interferometry, vol. 2447, pp. 228-239, Orlando, FL, April 1995.
- [3] R. A. Laskin, “Technology for Space Optical Interferometry,” Proceedings of the 33rd Aerospace Sciences Meeting and Exhibit, AIAA vol 95-0825, Reno, NV, January 1995.
- [4] J. W. Melody, G. W. Neat, “Integrated Modeling Methodology Validation Using the Micro-Precision Interferometer Testbed,” Proceedings of the 35th IEEE Conference on Decision and Control, Kobe, Japan, December 1996.
- [5] M. Milman, *et al.*, “Integrated Modeling of Optical Systems User’s Manual, Release 2.0,” JPL D-13040, November 15, 1995.
- [6] D. Redding, “Controlled Optics Modelling Package User Manual, Release 1.0,” JPL D-9816, June 1, 1992.
- [7] G. W. Neat, L. F. Sword, B. E. Hines, and R. J. Calvet, “Micro-Precision Interferometer Testbed: End-to-End System Integration of Control Structure Interaction Technologies,” Proceedings of the SPIE Symposium on OE/Aerospace, Science and Sensing, Conference on Spaceborne Interferometry, vol. 1817, pp. 9-103, Orlando, FL, April 1993.
- [8] B. E. Hines, “Optical Design Issues for the Micro-Precision Interferometer Testbed for Space-Based Interferometry,” Proceedings of the SPIE Symposium on OE/Aerospace, Science and Sensing, Conference on Spaceborne Interferometry, vol. 1947, pp. 114-125, Orlando, FL, April 1995.
- [9] G. W. Neat, J. F. O’Brien, N. M. Nerheim, R. J. Calvet, H. Singh, and S. Shaklan, “Micro-Precision Interferometer Testbed: First Stabilized Stellar Fringes,” Proceedings of the SPIE International Symposium on AeroSense, Conference on Spaceborne Interferometry II, vol. 2477, pp. 104-115, Orlando, FL, April 1995.